

# Network-level structural covariance in the developing brain

Brandon A. Zielinski, Efstathios D. Gennatas, Juan Zhou, and William W. Seeley<sup>1</sup>

Department of Neurology, University of California, San Francisco, CA 94143-0114

Edited by Marcus E. Raichle, Washington University of St. Louis, St. Louis, MO, and approved September 14, 2010 (received for review April 2, 2010)

**Intrinsic or resting state functional connectivity MRI and structural covariance MRI have begun to reveal the adult human brain's multiple network architectures. How and when these networks emerge during development remains unclear, but understanding ontogeny could shed light on network function and dysfunction. In this study, we applied structural covariance MRI techniques to 300 children in four age categories (early childhood, 5–8 y; late childhood, 8.5–11 y; early adolescence, 12–14 y; late adolescence, 16–18 y) to characterize gray matter structural relationships between cortical nodes that make up large-scale functional networks. Network nodes identified from eight widely replicated functional intrinsic connectivity networks served as seed regions to map whole-brain structural covariance patterns in each age group. In general, structural covariance in the youngest age group was limited to seed and contralateral homologous regions. Networks derived using primary sensory and motor cortex seeds were already well-developed in early childhood but expanded in early adolescence before pruning to a more restricted topology resembling adult intrinsic connectivity network patterns. In contrast, language, social-emotional, and other cognitive networks were relatively undeveloped in younger age groups and showed increasingly distributed topology in older children. The so-called default-mode network provided a notable exception, following a developmental trajectory more similar to the primary sensorimotor systems. Relationships between functional maturation and structural covariance networks topology warrant future exploration.**

childhood | children | connectivity | development | neuroimaging

Large-scale networks organize brain function (1), and defining human network architecture has become a major goal of neuroscience research. Network-sensitive imaging tools have invigorated these efforts, most notably resting state or intrinsic connectivity network (ICN) functional magnetic resonance imaging (fMRI). This technique, which correlates low frequency (<0.1 Hz) blood oxygen level-dependent (BOLD) signal fluctuations across distributed regions, has delineated consistent, anatomically predictable networks relating to sensory, motor, language, social-emotional, and cognitive functions (2–9). Furthermore, ICN connectivity strength has been shown to impact human behaviors, whether those behaviors are measured inside (10, 11) or outside (8) the scanner. Building on the ICN approach, several groups have mapped whole-brain correlations in gray matter volume across subjects (12–16). In our recent work in healthy adults (14), these structural covariance networks (SCNs) were shown to recapitulate the canonical ICN topologies, suggesting that SCNs might serve as a measure of network integrity for cross-sectional group studies.

To date, most network mapping studies in humans have focused on healthy or diseased adult populations, leaving much to be learned about the assembly of large-scale networks during development. The human brain undergoes profound global and regional changes throughout childhood (17–19). Overall brain volume achieves 80–90% of its lifetime maximum by 2 y of age (20), whereas in many regions gray matter volumes peak in infancy before undergoing variable rates of decline throughout adolescence (21–23). In contrast, myelination continues to progress from posterior to anterior throughout adolescence and well into young

adulthood (24, 25), and frontal myelination may continue beyond this age (19). These considerations suggest that the anatomical scaffolding for large-scale functional integration may not emerge until adolescence, particularly for late-myelinating systems with robust frontal connectivity. Using ICN approaches in infants, Fransson et al. (26) documented five ICNs reminiscent of networks seen in adults, although these infant ICNs seemed less robust and extensive. Other work suggests that some ICNs remain rudimentary in young children and undergo considerable subsequent modification (27, 28). Recent graph theoretical analyses of ICN and diffusion tensor imaging data suggest that children may move through distinct connectivity milestones en route to a mature adult pattern (29–31). Structural imaging data, although widely available, have been underused in the study of brain networks and provide a potential window into childhood development. One previous developmental study used structural covariance approaches (32) to show that cortical thickness in Broca's area correlates with thickness in superior temporal cortex. Moreover, this language system structural correlation becomes stronger throughout the age range of expected increases in language competency, suggesting that SCN maturation may have functional significance. However, to date, no study has explored the full complement of SCNs in children or examined how SCNs evolve throughout distinct developmental stages.

In this study, we used SCN mapping to investigate eight large-scale networks in 300 healthy children aged 5–18 y (Table 1), drawing from a large pediatric MRI repository (33). We hypothesized that childhood SCNs would reflect ICNs previously described in children and adults and would emerge following distinct age-related developmental trajectories. More specifically, we hypothesized that SCNs related to late-myelinating rostral cortices, including those subserving language, social-emotional, and executive control functions, would show the most protracted maturation, continuing to develop through late adolescence.

## Results

To survey the broad network landscape, including systems relating to sensory, motor, language, social-emotional, and cognitive functions, we used seed-based structural covariance analyses (14) to map eight distinct SCNs across four age groups (Figs. 1–3). Seeds (*Materials and Methods*) were chosen from networks widely replicated in the ICN literature, including the primary visual, auditory, and motor systems (2–4, 34), language-related networks subserving speech and semantics (8, 14, 35), and integrative systems related to salience processing (8), executive control (4, 8), and episodic memory [the so-called default-mode network (DMN)] (4–7). SCNs resulting from the eight seed-based statistical para-

Author contributions: B.A.Z. and W.W.S. designed research; B.A.Z. and E.D.G. performed research; B.A.Z., E.D.G., J.Z., and W.W.S. contributed new reagents/analytic tools; B.A.Z., E.D.G., and J.Z. analyzed data; and B.A.Z. wrote the paper.

The authors declare no conflict of interest.

This article is a PNAS Direct Submission.

<sup>1</sup>To whom correspondence should be addressed. E-mail: wseeley@memory.ucsf.edu.

This article contains supporting information online at [www.pnas.org/lookup/suppl/doi:10.1073/pnas.1003109107/-DCSupplemental](http://www.pnas.org/lookup/suppl/doi:10.1073/pnas.1003109107/-DCSupplemental).



childhood (Fig. 2A). The left inferior frontal gyrus, pars opercularis (IFGo; containing Broca's area) seed anchored bilateral IFGo and ipsilateral dorsal anterior insula covariance in group 1, which expanded to include bilateral dorsal anterior insulae in group 2, expanded further to include dorsolateral prefrontal cortex in group 3, and expanded further still to include more extensive frontal regions, posterior superior temporal gyrus (Wernicke's area), and frontoparietal sensorimotor and cingulate motor areas in group 4. A left temporal pole seed, chosen to map a network related to semantic knowledge (37, 38), covaried in group 1 with ipsilateral amygdala, contralateral temporal pole, and bilateral inferior temporal cortex. This pattern expanded to include bilateral insular regions in group 2 and contralateral amygdala, anterior cingulate, medial and lateral orbitofrontal, and frontopolar regions in group 3. Group 4 showed extensive inferior, mesial, and superior temporal and bilateral amygdalar, insular, orbitofrontal, and cingulate covariance, reflecting a previously identified adult ICN/SCN (14). Together, these findings suggest that language-related speech and semantic networks undergo continued expansion throughout childhood, with increasingly long-range covariance in early adolescence that progresses throughout the teenage years. The language-related patterns were reflected quantitatively by similar stage-wise increases in the number of significantly correlated voxels (Fig. 2B).

**Saliency, Executive Control, and Default-Mode Networks.** To assess networks associated with nonlinguistic social-emotional and cognitive functions, we measured structural covariance within an anterior cingulate-fronto-insular (FI) network related to saliency processing (8), a dorsolateral fronto-parietal network critical for executive control and working memory (8), and a posterior cingulo-temporo-parietal DMN related to episodic memory, visual imagery, and mentalizing (7). Strikingly, the saliency network and executive control network showed limited covariance patterns throughout initial stages of childhood, with far more distributed structural covariance in late adolescence (Fig. 3A). Specifically, the right frontoinsula (a major node within the saliency network) anchored covariance maps that included bilateral fronto-insular

and orbitofrontal regions in group 1 and bilateral insular, anterior cingulate cortex, and frontopolar regions in group 2. This SCN underwent significant extension in group 3 to include most of the medial frontal wall and bilateral insular cortex. In group 4, a robust and nearly contiguous SCN emerged comprised of extensive lateral and medial frontal, anterior cingulate, and anterior temporal cortices as well as bilateral amygdala. A seed in right dorsolateral prefrontal cortex (DLPFC; a major node within the executive control network) produced arguably the latest-maturing SCN, with only seed autocorrelation in groups 1 and 2 and contralateral DLPFC covariance in group 3. A much more extensive bifrontal covariance emerged in group 4, however, extending to dorsal anterior cingulate cortex, ventrolateral prefrontal cortex, and premotor areas. Right angular gyrus, a seed used to derive the DMN (14), showed limited covariance with contralateral angular gyrus in groups 1 and 2 with the addition of lateral temporal regions in group 3. More extensive bilateral lateral temporal and posterior cingulate covariance emerged in group 4. Somewhat unexpectedly, the DMN showed a peak voxel count in group 3 (Fig. 3B), resembling the pattern seen in the primary sensory and motor networks (Fig. 1B).

**Statistical Validation of Observed SCN Trajectory Profiles.** Noting distinct domain-related SCN trajectories (Figs. 1–3), we sought additional statistical support for these observations by modeling peak and prune and cumulative growth trajectory patterns for each of our SCNs (*Materials and Methods*). These follow-up analyses identified brain regions whose seed-based covariance conformed to each of the two trajectory patterns across age groups (Table S1). Overall, primary sensory and motor seeds showed covariance with several regions that significantly followed a peak and prune covariance trajectory model but few regions that significantly followed a cumulative growth trend. Conversely, seeds for the language-related, social-emotional, and executive control networks significantly covaried with numerous regions fitting the cumulative growth model, but only one region in one network conformed to a peak and prune trajectory. Only the DMN defied these catego-

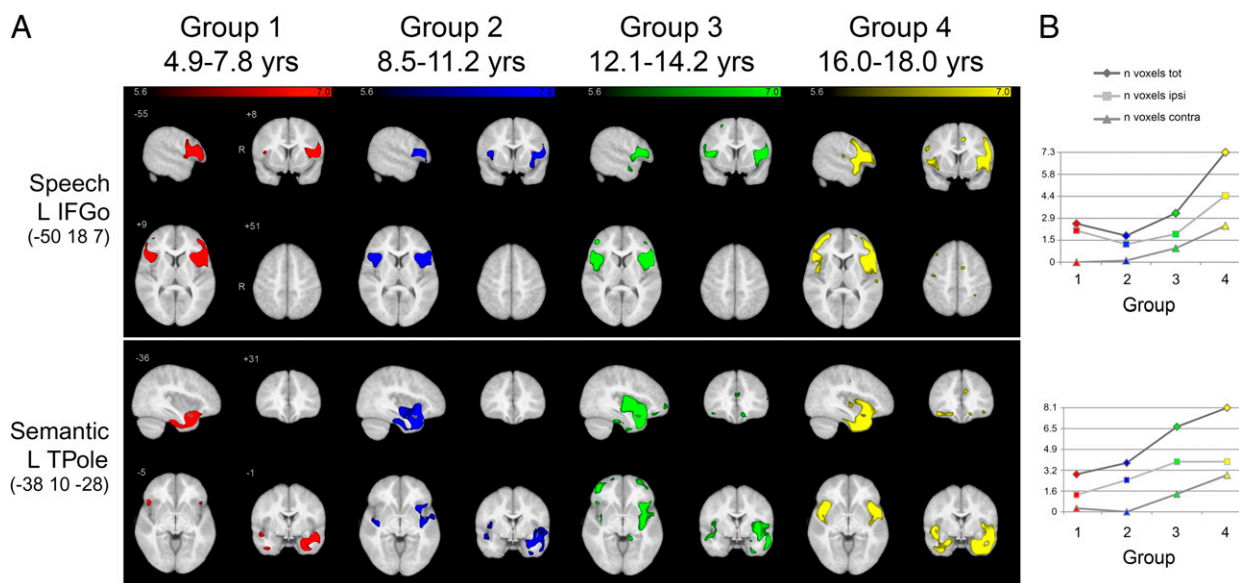


**Fig. 2.** Age-related differences in language-related speech and semantic networks. (A) Statistical maps depict brain regions in which gray matter intensity covaried with that of the seed ROI in each group. Structural covariance networks seem less well-developed at early ages, with subsequent persistent expansion throughout childhood to a peak level of large-scale distribution in group 4. scMRI data are z-statistic maps ( $P < 0.001$ , FWE-corrected) displayed on the custom average T1 template of all subjects. The left side of the image corresponds to the right side of the brain. (B) Plots of voxel counts by group indicate covariance expansion throughout childhood. The y-axis scale is voxel number ( $\times 10^4$ ) from associated statistical maps. IFGo, inferior frontal gyrus, pars opercularis; L, left; TPole, temporal pole.

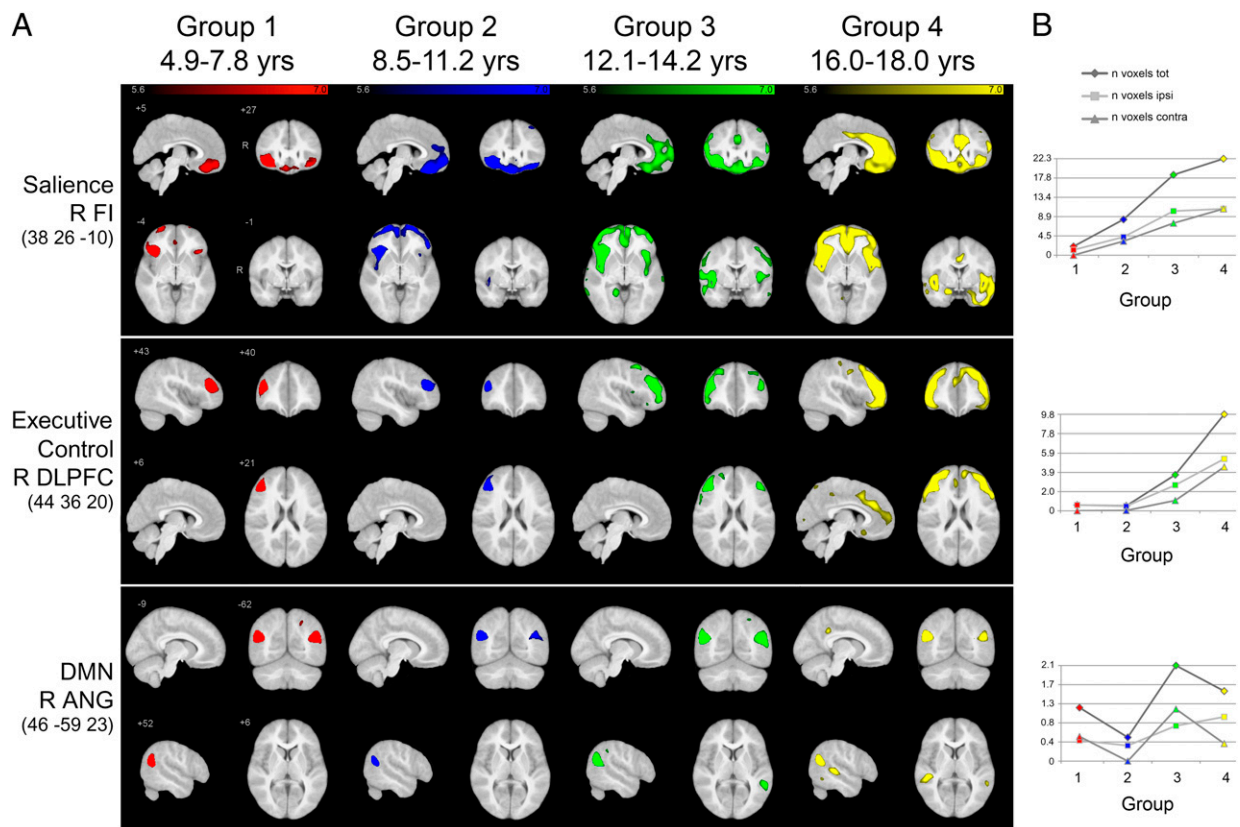


**Fig. 3.** Age-related differences in salience, executive control, and default-mode networks. (A) Statistical maps depict brain regions in which gray matter intensity covaried with that of the seed ROI in each group. Structural covariance networks seem poorly developed at early ages, with early covariance largely restricted to autocorrelation and contralateral homotopic regions. Subsequent persistent expansion continued throughout childhood, with expansion in adolescence within salience and executive control networks. The default-mode network (DMN) shows significant expansion in group 3 before restriction in group 4, similar to the pattern seen in primary sensory and motor networks. sCMRI data are z-statistic maps ( $P < 0.001$ , FWE) displayed on the custom average T1 template of all subjects. The left side of the image corresponds to the right side of the brain. (B) Plots of voxel counts by group indicate volume expansion throughout childhood, with noted late contraction within the DMN. The y-axis scale is voxel number ( $\times 10^4$ ) from associated statistical maps. ANG, angular gyrus; DLPFC, dorsolateral prefrontal cortex; FI, frontoinsula; R, right.

rizations, possibly reflecting the complex architecture of this network (*Discussion*). Importantly, the observed network trajectory signatures (Figs. 1B, 2B, and 3B) proved robust to experimental variations in statistical thresholding (Fig. S1).

**Laterality and Sex Effects on SCNs.** Recent studies suggest that structural hemispheric asymmetries may emerge during specific phases of child development (18, 19, 22, 24, 39). Although the present study was not designed to address laterality effects, we performed a preliminary investigation of these issues by generating SCNs and voxel counts using seeds contralateral to those first analyzed (Figs. 1–3). The contralateral seeds produced SCNs that largely mirrored our main findings, resulting in consistent SCN trajectory signatures (Fig. S2).

Reported sex differences in childhood brain maturation (40, 41) prompted us to consider similar differences in SCN development. Therefore, we divided each age group by sex, generated sex-specific SCN maps, and plotted corresponding voxel count trajectories for three SCNs, one from each of the three broad functional domains (Fig. S3). We chose the speech (L IFGo) and salience (R FI) networks in light of the view held by some authors that these cognitive domains may mature earlier in females (42–44), and we included the primary auditory [R Heschl’s gyrus (HG)] network without specific a priori predictions. In general, voxel plot trajectory graphs (Fig. S3) depict earlier network expansion in females, particularly for speech (IFGo) and salience (FI) networks. Direct statistical contrasts between males and females at each age suggested more

nuanced sex differences (Table S2), underscoring the need for future studies designed to address this issue. Overall, however, these data suggest subtle but compelling network topology and trajectory differences between males and females, consistent with the existing literature (40–42).

### Discussion

This study characterized eight SCNs in children at distinct developmental stages. Seed gray matter regions drawn from known ICNs anchored discrete SCN topologies, revealing structural covariance among regions that make up large-scale functional networks. As shown previously in adults (14), SCNs in children strongly recapitulated the consistent adult ICNs from which the seed regions were derived. Moreover, age-related changes within each network suggested that SCNs follow distinct developmental trajectories that depend, at least in part, on the broad functional domain subserved by the network. The findings build on previous work (18, 32), which identified system-specific cortical thickness trajectories throughout childhood. In contrast, we used network analyses to show how neural systems build large-scale structural covariance during development. The findings suggest that SCN approaches provide a powerful tool for understanding human brain maturation.

Our data can be viewed against the backdrop of previous ICN fMRI studies in children, which suggest that rudimentary ICNs emerge at early ages (26–28), whereas more robust large-scale functional coherence may not develop until adolescence as the

brain matures from a local to more distributed covariance topology (29, 30, 45). Specifically, Fransson et al. (26) reported well-developed primary sensory and motor ICNs in infants, but only a sparse DMN-like ICN was identified at this age. Another study (28) reported a partial DMN-like ICN at 2 wk of age that developed into a more mature network by 2 y of age. Using more quantitative indices of ICN strength, however, Fair et al. (27) reported markedly less well-developed DMN connectivity in 7- to 9-y-old children compared with adults, especially within hallmark posterior regions. Although ICN and SCN results should only be compared with caution, the late childhood SCN maturation shown here suggests that distributed SCNs may not be an inherent property of the human brain but instead may arise after a period of functional coactivation.

Our data further suggest that a network's developmental trajectory depends on its functional specialization. For example, consistent with earlier primary sensory and motor system ontogeny, relatively mature SCNs anchored by primary visual, auditory, and motor cortex seeds were present in 5- to 7-y-old children. In early adolescence, these networks exhibited a burst of more distributed covariance before pruning in late adolescence to an adult-like ICN pattern. In contrast, language-related, salience, and executive control networks blossomed later, continuing to expand through late adolescence, a time when frontal myelination begins to mature and children approach readiness for independent survival. Unexpectedly, the DMN's trajectory most closely resembled the patterns seen among primary sensory and motor systems. Nonetheless, even in late adolescents, the emerging posterior DMN elements (bilateral angular gyrus, middle temporal gyrus, and posterior cingulate cortex) lacked covariance with rostromedial frontal regions that form a major node within ICN renderings of the DMN in adults (5–7, 46) and inconsistently in children (26–28). This finding may relate to the DMN's complex composition, perhaps made up of multiple subnetworks (46, 47), including an anterior subsystem not detected in our analyses. Future studies are needed to resolve how DMN subnetworks differ in their developmental trajectories.

Although not designed to address laterality- or sex-based differences in SCN development, this study suggests that SCN techniques may provide important insights into these issues. Overall, seed laterality exerted little influence on network ontogeny, perhaps reflecting the largely symmetric, distributed patterns seen in adult ICN and SCN renderings (2, 4, 5, 14). Primary visual cortex provided a notable exception, with the left calcarine sulcus-derived SCN blossoming later than its right hemisphere counterpart, a finding that converges with the late adolescent emergence of leftward visual system cortical thickness asymmetry (39). Sex contrasts were underpowered in the present study because of sample size constraints, and resulting sex differences should be interpreted with caution. Nonetheless, the SCN approach revealed earlier expansion of frontally seeded language and social-emotional network covariance in females, consistent with previous suggestions that females mature earlier in these domains (39). Future studies may help clarify whether SCNs show the age-dependent sexual dimorphism suggested by previous work using different measures (41, 44).

Little is known about the biological relationships between ICN and SCN architectures. We have speculated that SCNs reflect shared long-term trophic influences within functionally synchronous systems, common neurodevelopmental blueprints for axonal guidance and neuronal migration, or a combination of these factors (14). Recent studies have begun to explore the structural underpinnings of ICNs using white matter diffusion tractography to identify anatomical connections between functionally correlated regions (48, 49). Future studies combining functional and structural correlation approaches may help clarify the interdependence of these forms of network covariance. Multimodal analyses could delineate the timing of ICN vs. SCN ontogeny,

whereas longitudinal studies may help clarify how network covariance relates to the emergence of core competencies during childhood.

Whether age-specific structural covariance patterns enable or simply reflect human network functioning remains unknown. Previous studies have documented age-dependent patterns of regional cortical thickness in healthy children (18, 50), and structural changes have been associated with practice and learning (51–53) as well as with aging and disease (54, 55). A comprehensive, data-driven approach to human connectomic mapping (56) may provide a framework for understanding normal childhood development as well as neurodevelopmental (31) and age-related disorders (14) that impact network function.

## Methods

**Subjects and MRI Methods.** Deidentified data were obtained from the National Institutes of Health (NIH) MRI Study of Normal Brain Development's Pediatric MRI Data Repository (33). This multisite study includes T1 MRI scans of 432 normal children between the ages of 4.5 and 21 y (no older than 18 y at enrollment). Further details regarding MRI methods, demographics, inclusion and exclusion criteria, and other technical specifications have been published (33). Briefly, MR images were acquired using standard 1.5 T MRI scanners (GE; Siemens). Whole-brain T1-weighted image datasets were acquired using standard techniques (time to repetition median = 23 ms, time to echo median = 10 ms, matrix median =  $256 \times 256 \times 124$ , and median voxel volume =  $1.32 \text{ mm}^3$ ). We used all nonduplicate high-quality scans available in the database from right-handed subjects to select our study sample. Based on estimates of statistical power from previous structural covariance MRI (scMRI) studies (8), we constructed four sex-matched groups ( $n = 75$ , 34 males and 41 females) by first selecting the 75 oldest (group 4) subjects. We then selected the 75 youngest (Group 1) subjects, matching for sex. We divided the remaining subjects into two equally sized groups before selecting 75 nonduplicate subjects surrounding the respective group means, again matching for sex (groups 3 and 4). Resulting group characteristics are shown in Table 1.

**Data Analysis.** We created customized image analysis templates by normalizing, segmenting, and averaging T1 images using SPM5 according to a recently proposed processing pipeline (57, 58). First, images were transformed into standard space using a 12-parameter affine-only linear transformation and segmented into three tissue classes representing gray matter, white matter, and cerebrospinal fluid. Smoothly varying intensity changes as well as artifactual intensity alterations as a result of the normalization step were corrected for using a standard modulation algorithm within SPM5. The resulting segmented maps were then smoothed using a 12-mm full-width at half-maximum Gaussian kernel. To study network structural covariance, we derived gray matter intensities using 4-mm-radius spherical seed regions of interest (ROIs) chosen using previously published ICN peak foci from the adult ICN literature and adjusted to our childhood template using relevant anatomical landmarks to avoid seed placement too near the pial surface. Seed ROIs were selected within right calcarine sulcus (primary visual cortex) (59), right Heschl's gyrus (primary auditory cortex) (60), right precentral gyrus (primary motor cortex) (61), left inferior frontal gyrus, pars opercularis (Broca's area) (14), left temporal pole (14), right frontoinsular cortex (14), right dorsolateral prefrontal cortex (8), and right angular gyrus (14). These regions anchor the visual, auditory, sensorimotor, speech, semantic, salience, executive control, and default-mode networks, respectively (4, 7, 8, 14). We performed separate condition-by-covariate analyses for each seed region in which the mean seed gray matter intensity was the covariate of interest and age group was the grouping variable. This design enabled us to determine the whole-brain patterns of seed-based structural covariance in each age group. Resulting correlation maps were thresholded at  $P < 0.001$ , corrected for FWE, and displayed on the normalized pediatric brain template to allow qualitative comparisons between age groups. To quantify differences in developmental trajectory across networks, we calculated the total number of significant ipsilateral, contralateral, and whole-brain voxels and plotted these by age group (Figs. 1–3).

Follow-up analyses sought statistical support for the domain-related voxel plot trajectories observed in Figs. 1B, 2B, and 3B by modeling the proposed primary sensory and motor trajectories as peak and prune ( $-1 - 1 + 3 - 1$ ) contrasts and the language-related and cognitive trajectories as cumulative growth ( $-1 - 0.5 + 0.5 + 1$ ) contrasts (Table S1). Both contrasts were applied to each seed to identify regions that significantly conformed to each model ( $P < 0.001$ , uncorrected). These analyses were inclusively masked by the largest

group map (group 3 for peak and prune and group 4 for cumulative growth contrasts), with the mask thresholded more generously ( $P < 0.01$ , FWE-corrected) to avoid overly constraining the search volume.

Additional analyses using contralateral seeds (Fig. S2) were performed by changing the sign on each seed's  $x$  coordinate and following otherwise identical procedures to those used in generating the results shown in Figs. 1–3. Likewise, sex effects were examined by dividing each group by sex within otherwise identical statistical models. Sex-specific group SCNs were derived for voxel plot trajectories (Fig. S3) using a less-stringent statistical threshold

given the lower sample sizes ( $P < 0.01$ , FWE-corrected). Linear group contrasts sought regional head-to-head sex differences in seed covariance at each age ( $P < 0.001$ , uncorrected, inclusively masked to the group average map at  $P < 0.05$ , uncorrected) (Table S2).

**ACKNOWLEDGMENTS.** This work was supported by the Larry L. Hillblom Foundation, the Pediatric National Institutes of Health MRI Data Repository, and a University of California San Francisco Clinical and Translational Science Institute Resident Research Award (to B.A.Z.).

- Mesulam MM (1998) From sensation to cognition. *Brain* 121:1013–1052.
- Beckmann CF, DeLuca M, Devlin JT, Smith SM (2005) Investigations into resting-state connectivity using independent component analysis. *Philos Trans R Soc Lond B Biol Sci* 360:1001–1013.
- Biswal B, Yetkin FZ, Haughton VM, Hyde JS (1995) Functional connectivity in the motor cortex of resting human brain using echo-planar MRI. *Magn Reson Med* 34:537–541.
- Damoiseaux JS, et al. (2006) Consistent resting-state networks across healthy subjects. *Proc Natl Acad Sci USA* 103:13848–13853.
- Fox MD, et al. (2005) The human brain is intrinsically organized into dynamic, anticorrelated functional networks. *Proc Natl Acad Sci USA* 102:9673–9678.
- Fransson P (2005) Spontaneous low-frequency BOLD signal fluctuations: An fMRI investigation of the resting-state default mode of brain function hypothesis. *Hum Brain Mapp* 26:15–29.
- Greicius MD, Krasnow B, Reiss AL, Menon V (2003) Functional connectivity in the resting brain: A network analysis of the default mode hypothesis. *Proc Natl Acad Sci USA* 100:253–258.
- Seeley WW, et al. (2007) Dissociable intrinsic connectivity networks for salience processing and executive control. *J Neurosci* 27:2349–2356.
- Zhang D, et al. (2008) Intrinsic functional relations between human cerebral cortex and thalamus. *J Neurophysiol* 100:1740–1748.
- Fox MD, Snyder AZ, Vincent JL, Raichle ME (2007) Intrinsic fluctuations within cortical systems account for intertrial variability in human behavior. *Neuron* 56:171–184.
- Hesselmann G, Kell CA, Eger E, Kleinschmidt A (2008) Spontaneous local variations in ongoing neural activity bias perceptual decisions. *Proc Natl Acad Sci USA* 105:10984–10989.
- Liu Y, et al. (2008) Disrupted small-world networks in schizophrenia. *Brain* 131:945–961.
- Bassett DS, et al. (2008) Hierarchical organization of human cortical networks in health and schizophrenia. *J Neurosci* 28:9239–9248.
- Seeley WW, Crawford RK, Zhou J, Miller BL, Greicius MD (2009) Neurodegenerative diseases target large-scale human brain networks. *Neuron* 62:42–52.
- He Y, Chen ZJ, Evans AC (2007) Small-world anatomical networks in the human brain revealed by cortical thickness from MRI. *Cereb Cortex* 17:2407–2419.
- Mechelli A, Friston KJ, Frackowiak RS, Price CJ (2005) Structural covariance in the human cortex. *J Neurosci* 25:8303–8310.
- Giedd JN, et al. (1999) Brain development during childhood and adolescence: A longitudinal MRI study. *Nat Neurosci* 2:861–863.
- Shaw P, et al. (2008) Neurodevelopmental trajectories of the human cerebral cortex. *J Neurosci* 28:3586–3594.
- Sowell ER, Thompson PM, Toga AW (2004) Mapping changes in the human cortex throughout the span of life. *Neuroscientist* 10:372–392.
- Pfefferbaum A, et al. (1994) A quantitative magnetic resonance imaging study of changes in brain morphology from infancy to late adulthood. *Arch Neurol* 51:874–887.
- Matsuzawa J, et al. (2001) Age-related volumetric changes of brain gray and white matter in healthy infants and children. *Cereb Cortex* 11:335–342.
- Gogtay N, et al. (2004) Dynamic mapping of human cortical development during childhood through early adulthood. *Proc Natl Acad Sci USA* 101:8174–8179.
- Knickmeyer RC, et al. (2008) A structural MRI study of human brain development from birth to 2 years. *J Neurosci* 28:12176–12182.
- Paus T, et al. (1999) Structural maturation of neural pathways in children and adolescents: In vivo study. *Science* 283:1908–1911.
- Bartzokis G, et al. (2001) Age-related changes in frontal and temporal lobe volumes in men: A magnetic resonance imaging study. *Arch Gen Psychiatry* 58:461–465.
- Fransson P, et al. (2007) Resting-state networks in the infant brain. *Proc Natl Acad Sci USA* 104:15531–15536.
- Fair DA, et al. (2008) The maturing architecture of the brain's default network. *Proc Natl Acad Sci USA* 105:4028–4032.
- Gao W, et al. (2009) Evidence on the emergence of the brain's default network from 2-week-old to 2-year-old healthy pediatric subjects. *Proc Natl Acad Sci USA* 106:6790–6795.
- Fair DA, et al. (2007) Development of distinct control networks through segregation and integration. *Proc Natl Acad Sci USA* 104:13507–13512.
- Fair DA, et al. (2009) Functional brain networks develop from a "local to distributed" organization. *PLoS Comput Biol* 5:e1000381.
- Church JA, et al. (2009) Control networks in paediatric Tourette syndrome show immature and anomalous patterns of functional connectivity. *Brain* 132:225–238.
- Lerch JP, et al. (2006) Mapping anatomical correlations across cerebral cortex (MACACC) using cortical thickness from MRI. *Neuroimage* 31:993–1003.
- Evans AC; Brain Development Cooperative Group (2006) The NIH MRI study of normal brain development. *Neuroimage* 30:184–202.
- De Luca M, Beckmann CF, De Stefano N, Matthews PM, Smith SM (2006) fMRI resting state networks define distinct modes of long-distance interactions in the human brain. *Neuroimage* 29:1359–1367.
- Davis MH, Johnsrude IS (2003) Hierarchical processing in spoken language comprehension. *J Neurosci* 23:3423–3431.
- Mesulam M (2008) Representation, inference, and transcendent encoding in neurocognitive networks of the human brain. *Ann Neurol* 64:367–378.
- Scott SK, Leff AP, Wise RJ (2003) Going beyond the information given: A neural system supporting semantic interpretation. *Neuroimage* 19:870–876.
- Rogers TT, et al. (2006) Anterior temporal cortex and semantic memory: Reconciling findings from neuropsychology and functional imaging. *Cogn Affect Behav Neurosci* 6:201–213.
- Shaw P, et al. (2009) Development of cortical asymmetry in typically developing children and its disruption in attention-deficit/hyperactivity disorder. *Arch Gen Psychiatry* 66:888–896.
- Giedd JN (2004) Structural magnetic resonance imaging of the adolescent brain. *Ann N Y Acad Sci* 1021:77–85.
- Lenroot RK, Giedd JN (2010) Sex differences in the adolescent brain. *Brain Cogn* 72:46–55.
- Lenroot RK, et al. (2007) Sexual dimorphism of brain developmental trajectories during childhood and adolescence. *Neuroimage* 36:1065–1073.
- Bornstein MH, Painter KM, Park J (2002) Naturalistic language sampling in typically developing children. *J Child Lang* 29:687–699.
- Blakemore SJ (2008) The social brain in adolescence. *Nat Rev Neurosci* 9:267–277.
- Supekar K, Musen M, Menon V (2009) Development of large-scale functional brain networks in children. *PLoS Biol* 7:e1000157.
- Uddin LQ, Kelly AM, Biswal BB, Xavier Castellanos F, Milham MP (2009) Functional connectivity of default mode network components: Correlation, anticorrelation, and causality. *Hum Brain Mapp* 30:625–637.
- Andrews-Hanna JR, Reidler JS, Sepulcre J, Poulin R, Buckner RL (2010) Functional-anatomic fractionation of the brain's default network. *Neuron* 65:550–562.
- Honey CJ, et al. (2009) Predicting human resting-state functional connectivity from structural connectivity. *Proc Natl Acad Sci USA* 106:2035–2040.
- Greicius MD, Supekar K, Menon V, Dougherty RF (2009) Resting-state functional connectivity reflects structural connectivity in the default mode network. *Cereb Cortex* 19:72–78.
- Shaw P, et al. (2006) Intellectual ability and cortical development in children and adolescents. *Nature* 440:676–679.
- Ilg R, et al. (2008) Gray matter increase induced by practice correlates with task-specific activation: A combined functional and morphometric magnetic resonance imaging study. *J Neurosci* 28:4210–4215.
- Mechelli A, et al. (2004) Neurolinguistics: Structural plasticity in the bilingual brain. *Nature* 431:757.
- Draganski B, et al. (2004) Neuroplasticity: Changes in grey matter induced by training. *Nature* 427:311–312.
- Brickman AM, Habek C, Zarahn E, Flynn J, Stern Y (2007) Structural MRI covariance patterns associated with normal aging and neuropsychological functioning. *Neurobiol Aging* 28:284–295.
- Bergfield KL, et al. (2010) Age-related networks of regional covariance in MRI gray matter: Reproducible multivariate patterns in healthy aging. *Neuroimage* 49:1750–1759.
- Biswal BB, et al. (2010) Toward discovery science of human brain function. *Proc Natl Acad Sci USA* 107:4734–4739.
- Wilke M, Holland SK, Altaye M, Gaser C (2008) Template-O-Matic: A toolbox for creating customized pediatric templates. *Neuroimage* 41:903–913.
- Altaye M, Holland SK, Wilke M, Gaser C (2008) Infant brain probability templates for MRI segmentation and normalization. *Neuroimage* 43:721–730.
- Wang K, et al. (2008) Spontaneous activity associated with primary visual cortex: A resting-state FMRI study. *Cereb Cortex* 18:697–704.
- Xiang HD, Fonteijn HM, Norris DG, Hagoort P (2010) Topographical functional connectivity pattern in the perisylvian language networks. *Cereb Cortex* 20:549–560.
- Lowe MJ, Mock BJ, Sorenson JA (1998) Functional connectivity in single and multislice echoplanar imaging using resting-state fluctuations. *Neuroimage* 7:119–132.